Bone 127 (2019) 324–333

Contents lists available at ScienceDirect

Bone

journal homepage: www.elsevier.com/locate/bone

Full Length Article

# Aberrant activation of Wnt signaling pathway altered osteocyte mineralization

Yinghong Zhou[c,d,g,i,1], Jinying Lin[a,b,i,1], Jin Shao[c,g,i], Qiliang Zuo[a,b,i], Shengfang Wang[c,g,i], Annalena Wolff[e], Dung Trung Nguyen[f], Llew Rintoul[e], Zhibin Du[c,g,i], Yuantong Gu[g,i], Yong Y. Peng[h], John A.M. Ramshaw[h,2], Xing Long[a,i,*], Yin Xiao[a,c,d,g,i,**]

[a] The State Key Laboratory Breeding Base of Basic Science of Stomatology (Hubei-MOST) & Key Laboratory of Oral Biomedicine Ministry of Education, School & Hospital of Stomatology, Wuhan University, Wuhan 430079, China
[b] Department of Implantology, Affiliated Stomatological Hospital of Xiamen Medical College, Fujian 361000, China
[c] Institute of Health and Biomedical Innovation, Queensland University of Technology (QUT), Brisbane, QLD 4059, Australia
[d] Key Laboratory of Oral Medicine, Guangzhou Institute of Oral Disease, Stomatology Hospital of Guangzhou Medical University, Guangzhou 51050, China
[e] Central Analytical Research Facility, Institute for Future Environments, Queensland University of Technology (QUT), Brisbane, QLD 4000, Australia
[f] Department of Engineering and Computer Science, Seattle Pacific University, Seattle, WA 98119, USA
[g] School of Chemistry, Physics and Mechanical Engineering, Science and Engineering Faculty, Queensland University of Technology (QUT), Brisbane, QLD 4000, Australia
[h] CSIRO Manufacturing, Bayview Avenue, Clayton, VIC 3168, Australia
[i] The Australia-China Centre for Tissue Engineering and Regenerative Medicine (ACCTERM), Queensland University of Technology (QUT), Brisbane, QLD 4000, Australia

ARTICLE INFO

*Keywords:*
Osteocyte
Mineralization
Wnt/β-catenin
Dentin Matrix Protein 1 (DMP1)
Cell signaling
Osteogenesis

ABSTRACT

Mineralization of bone is a dynamic process, involving a complex interplay between cells, secreted macromolecules, signaling pathways, and enzymatic reactions; the dysregulation of bone mineralization may lead to serious skeletal disorders, including hypophosphatemic rickets, osteoporosis, and rheumatoid arthritis. Very few studies have reported the role of osteocytes — the most abundant bone cells in the skeletal system and the major orchestrators of bone remodeling in bone mineralization, which is owed to their nature of being deeply embedded in the mineralized bone matrix. The Wnt/β-catenin signaling pathway is actively involved in various life processes including osteogenesis; however, the role of Wnt/β-catenin signaling in the terminal mineralization of bone, especially in the regulation of osteocytes, is largely unknown. This research demonstrates that during the terminal mineralization process, the Wnt/β-catenin pathway is downregulated, and when Wnt/β-catenin signaling is activated in osteocytes, dendrite development is suppressed and the expression of dentin matrix protein 1 (DMP1) is inhibited. Aberrant activation of Wnt/β-catenin signaling in osteocytes leads to the spontaneous deposition of extra-large mineralized nodules on the surface of collagen fibrils. The altered mineral crystal structure and decreased bonding force between minerals and the organic matrix indicate the inferior integration of minerals and collagen. In conclusion, Wnt/β-catenin signaling plays a critical role in the terminal differentiation of osteocytes and as such, targeting Wnt/β-catenin signaling in osteocytes may serve as a potential therapeutic approach for the management of bone-related diseases.

## 1. Introduction

Bone mineralization is a complex process by which mineral crystals are deposited in an organized fashion onto the organic extracellular matrix (ECM). It is finely controlled by the interplay between cells, secreted macromolecules, signaling pathways, and enzymatic reactions. Osteocytes are a major cell type involved in this process; they are derived from the osteogenic lineage and account for 90% of all cells in

* Correspondence to: X. Long, The State Key Laboratory Breeding Base of Basic Science of Stomatology (Hubei-MOST) & Key Laboratory of Oral Biomedicine Ministry of Education, School & Hospital of Stomatology, Wuhan University, Wuhan 430079, China.
** Correspondence to: Y. Xiao, Institute of Health and Biomedical Innovation, Queensland University of Technology (QUT), Brisbane, QLD 4059, Australia.
*E-mail addresses:* yinghongzhou@qut.edu.au (Y. Zhou), jin.shao@connect.qut.edu.au (J. Shao), shengfang.wang@hdr.qut.edu.au (S. Wang), annalena.wolff@qut.edu.au (A. Wolff), nguyend16@spu.edu (D.T. Nguyen), l.rintoul@qut.edu.au (L. Rintoul), zhibin.du@qut.edu.au (Z. Du), yuantong.gu@qut.edu.au (Y. Gu), yong.peng@csiro.au (Y.Y. Peng), longxing@whu.edu.cn (X. Long), yin.xiao@qut.edu.au (Y. Xiao).
[1] YZ and JL contributed equally to this work and are joint first authors.
[2] Present address: Department of Surgery, St. Vincent's Hospital, University of Melbourne, VIC 3065, Australia.

https://doi.org/10.1016/j.bone.2019.06.027
Received 27 February 2019; Received in revised form 27 June 2019; Accepted 27 June 2019
Available online 28 June 2019

mature bone tissues. A mature osteocyte represents an osteoblast at a terminally differentiated stage that becomes progressively embedded within the lacunae of the mineralized matrix. As osteocytes are embedded within the matrix and further differentiate, they undergo a dramatic morphologic transformation and display multiple cytoplasmic dendritic processes from the cell body, passing through the bone matrix along narrow canals called canaliculi [1]. Through the elongated dendrites, osteocytes establish contact with other embedded osteocytes and cells on the bone surface; thus osteocytes are not merely passive, inactive cells that serve as place holders in the bone matrix according to previously suggested dogma, but act more as critical orchestrators of bone homeostasis [2]. This critical process is achieved by integrating mechanical loading and hormonal signals to maintain the balance between bone formation and resorption [1,3].

As osteocytes are one of the longest living cells in the body, the optimal function of the osteocyte network is extremely important for bone health [2]. However, it is quite challenging to harvest osteocytes for functional studies as these cells are deeply embedded within the mineralized bone matrix. IDG-SW3, a recently developed cell line that replicates osteoblast-to-late-osteocyte differentiation, is derived by crossing the DMP1-GFP transgenic mouse with the immortomouse, which expresses temperature sensitive SV40 large T antigen regulated by interferon gamma (IFN-γ) [4]. This cell line expresses early osteocyte markers such as E11, DMP1, Phex, and MEPE, as well as late osteocyte markers such as SOST and FGF-23. Thus, the IDG-SW3 cell line is a useful tool to study the transition from osteoblasts to osteocytes and the mechanisms for biomineralization, particularly with regards to ECM secretion, assembly, and mineralization.

Previous studies have revealed that a comprehensive signaling network is involved in mineralized tissue development and regeneration, among which the canonical Wnt/β-catenin signaling pathway plays a complex role, as it has various functions depending on the cell types and differentiation stages [5–8]. It has been reported that Wnt promotes bone formation by enhancing both the proliferation and differentiation of bone marrow stromal cells (BMSCs) [9,10]. β-Catenin, a central player in the canonical Wnt pathway, is critical for osteoblast differentiation [11,12], and has been demonstrated to promote the anti-osteoclastic activity of differentiated osteoblasts [12,13]. Wnt antagonists such as Dkk1, Dkk2, and sclerostin (SOST), are expressed at appreciable levels in osteocytes. Recent studies have demonstrated that the knockdown of β-catenin in osteocytes resulted in progressive bone loss in the appendicular and axial skeleton, providing direct proof of the important role of Wnt/β-catenin signaling in osteocytes in regulating bone mass [14]. However, the constitutive activation of β-catenin in osteocytes can increase cancellous bone mass, with decreased bone strength, suggesting a complicated role of Wnt/β-catenin signaling in bone biomineralization [15].

Although there is still a lack of direct data illustrating the effect of Wnt signaling on terminal bone mineralization due to the inaccessible location of osteocytes within the mineralized bone matrix, determination of osteocyte function *in vitro* has been greatly facilitated by the creation of immortalized osteocyte-like cell lines. By using IDG-SW3, a recently developed osteocyte cell line that expresses critical osteocyte-related markers, we were able to characterize the ultrastructural features of bone cell mineralization and were able to further investigate the role of Wnt signaling in the regulation of osteocyte mineralization.

## 2. Materials and methods

### 2.1. Cell culture

The murine IDG-SW3 (EKC001, Kerafast, USA) cell line was expanded in plates coated with rat tail type I collagen (0.2 mg/mL in 0.2 M acetic acid) under proliferative conditions at 33 °C in α-MEM (Gibco®, Thermo Fisher Scientific) containing 10% fetal bovine serum (FBS), penicillin (100 U/mL), streptomycin (50 μg/mL), and IFN-γ (50 U/mL) (Gibco®, Thermo Fisher Scientific). The IDG-SW3 cells were plated at a density of 80,000 cells/cm$^2$ under osteogenic differentiation conditions (at 37 °C in the aforementioned proliferation medium without IFN-γ, and supplemented with 50 μg/mL of ascorbic acid and 4 mM β-glycerophosphate) to induce their differentiation into osteocytes.

### 2.2. Collagen preparation

The differentiation process of IDG-SW3 cells is the same as that of primary osteocytes *in vivo*, especially in 3D, compared to 2D cultures; therefore, to further demonstrate the ability of IDG-SW3 cells to infiltrate and mineralize 3D substrates, the cells were seeded onto collagen sponges in some of the subsequent experiments [4]. Pepsin-soluble porcine collagen was prepared in accordance with standard methods [16]. For collagen sponge formation, collagen solution (5 mg/mL) prepared in 20 mM acetic acid was utilized. To stabilize the sponges, immediately before use, the pH of the collagen solution was adjusted to 7.2 using 2 M NaOH, and 10% *w/v* glutaraldehyde was immediately added, to achieve a final concentration of 0.5% w/v, followed by thorough mixing. Within 2 min of these additions, 0.4-mL aliquots of this solution were dispensed into wells of a 24-well tissue culture plate. After a further 15 min, these samples were frozen at −20 °C and subsequently freeze-dried. IDG-SW3 cells were then seeded onto the prefabricated collagen sponges at a density of $2 \times 10^4$ cells/collagen sponge and cultured in the respective growth medium or osteogenic medium, as described above, for two weeks prior to further analysis.

### 2.3. Activation of the Wnt signaling pathway

To activate the Wnt signaling pathway, Wnt3a-conditioned medium was prepared using a genetically modified murine cell line over-expressing L-Wnt3a (ATCC CRL-2647; American Type Culture Collection, Manassas, VA, USA); the protocol that we used was in accordance to previously published protocols [17,18]. The cell line was cultured according to the supplier's guidelines in a T75 flask with ATCC-formulated DMEM, supplemented with 10% *v*/v FBS and 0.4 mg/mL G418 (Sigma-Aldrich; Merck Millipore) to select Wnt3a-positive cells. The conditioned medium (CM) was prepared by splitting the cells in a 1:10 ratio in 10 mL of culture medium without G418, followed by incubation for 4 days. The first batch of the CM was obtained and filtered under sterile conditions, and 10 mL of fresh culture medium was added. The cells were cultured for an additional 3 days before the second CM batch was collected. The CM was aliquoted and then added to the aforementioned osteogenic medium for further experiments when needed. The working CM comprised a 1:1 mixture of the CM from the two batches.

### 2.4. Western blotting

Whole-cell lysates were collected for the western blotting analysis. A total of 15 μg of proteins from each sample was separated on SDS-PAGE gels; the protein bands were then transferred onto nitrocellulose membranes (Pall Corporation). After being blocked using Odyssey blocking buffer for 1 h (P/N 927-40000, LI-COR Biosciences), the membranes were incubated with primary antibodies against Wnt3a (1:1000, ab28472, Abcam), β-catenin (1:1000, #9581, Cell Signaling Technology), E11 (1:1000, ab10288, Abcam), DMP1 (1:1000, a kind gift from Professor Jerry Feng of the Texas A&M University College of Dentistry), and GAPDH (1:2000, ab8245, Abcam) overnight at 4 °C. The membranes were then incubated with anti-mouse/rabbit fluorescent-dye conjugated secondary antibodies at a dilution of 1:10000 for 1 h at room temperature. The protein bands were visualized using the Odyssey Infrared Imaging System (LI-COR Biosciences). The relative intensity of the protein bands was quantified using ImageJ software.

### 2.5. Immunofluorescence staining

The DMP1-GFP-positive cells during two weeks of osteogenic culture with or without the supplementation of Wnt3a medium were imaged using Nikon A1R confocal microscope. The nuclei were visualized using Hoechst 33342 solution (Thermo Fisher Scientific). To further confirm the active status of β-catenin, IDG-SW3 cells were seeded on 8-well chamber slides (177445, Lab-Tek) at a density of 4000 cells per well. After two weeks of osteogenic culture with or without Wnt3a stimulation, the cells were fixed with 4% paraformaldehyde (PFA) for 20 min at room temperature. The primary antibody against β-catenin (#9581, Cell Signaling Technology, 1:100) was diluted in PBST with 1% BSA at 4 °C overnight, followed by incubation with anti-rabbit IgG (H + L) Alex Fluor®488 (#4412, Cell Signaling Technology) at room temperature for 40 min to detect the primary antibodies. The slides were counterstained with DAPI (D1306, Thermo Fisher Scientific) and mounted with ProLong® Gold Antifade Reagent (P10144, Thermo Fisher Scientific).

### 2.6. Reverse transcription-quantitative polymerase chain reaction (RT-qPCR)

Total RNA was extracted using TRIzol® reagent (Thermo Fisher Scientific) to perform the reverse transcription-quantitative polymerase chain reaction (RT-qPCR). Complementary DNA was synthesized from 1 μg of total RNA using SensiFAST™ cDNA Synthesis Kit (Bioline Australia Pty Ltd.), following the manufacturer's instructions. RT-qPCR primers (Table 1) were designed using the cDNA sequences from the NCBI sequence database. SYBR™ Green PCR Master Mix (Thermo Fisher Scientific) was used to track the amplification process, and the target mRNA expression levels were assayed on the QuantStudio™ 7 Flex Real-Time PCR System (Thermo Fisher Scientific). Experiments were performed in triplicate. The mean cycle threshold (Ct) value of each target gene was normalized against the Ct value of the house keeping gene *GAPDH*.

### 2.7. Alizarin Red S staining and von Kossa staining

To visualize the mineral deposition, Alizarin Red S staining and von Kossa staining were performed as described previously [19,20]. After two weeks of osteogenic differentiation, the cells were stained with 1% Alizarin Red S (A5533, Sigma–Aldrich) solution (pH 4.2) for 20 min. After the removal of the unincorporated excess dye with distilled water, the mineralized nodules were labelled as red spots. For von Kossa staining, fixed cell culture samples were incubated with 5% silver nitrate solution (209139, Sigma-Aldrich) and exposed to UV light for 30 min. The unreacted silver salts were dissolved with 5% sodium thiosulfate solution and washed off with distilled water. Mineralized nodules were seen as dark brown to black spots. All samples were air-dried and images were captured using a phase contrast microscope (Nikon, Japan).

### 2.8. Scanning electron microscopy (SEM) imaging and analysis

The cell/collagen constructs or cells were cultured on 13-mm$^2$ coverslips in 24-well plates for 14 days with or without Wnt3a stimulation, and then rinsed with phosphate buffered saline (PBS); they were then fixed using 2.5% glutaraldehyde prepared in 0.1 M cacodylate buffer (pH 7.4) for 1 h. The cell cultures were post-fixed in 1% osmium tetroxide, and then dehydrated using a graded ethanol series (50%, 70%, 90%, and 100%) and dried with hemamethyldisilizene (HMDS). For morphological studies, the coverslips (with cell cultures) were attached to stubs and coated with a gold layer (10-nm thickness) by sputter deposition, and viewed with a FEG-SEM (Zeiss Sigma VP-FESEM) at an accelerating voltage of 10 kV. Carbon-coated samples were analyzed by energy dispersive X-ray spectroscopy (EDS) using a Zeiss Sigma VP Field Emission SEM operating at 10 kV and at a working distance of 10 mm. The atomic ratio between calcium and phosphorus (Ca/P) was calculated from five different nodules of each sample. Density-dependent color scanning electron micrographs (DDC-SEMs) were obtained according to a previously published protocol [21]. By using this technique, both topography and density could be simultaneously visualized in a single image. Images of the same region were first acquired in the in-lens mode and then using the backscatter mode. Both images were stacked using ImageJ software, and the in-lens images were assigned to the green channel, indicating a loose matrix, and the backscatter images were assigned to the red channel, indicating denser material.

**Table 1**
The primer sequences used for RT-qPCR.

| | |
|---|---|
| Fwd_*DMP1* | GCATCCTGCTCATGTTCCTTTG |
| Rev_*DMP1* | GAGCCAAATGACCCTTCCATTC |
| Fwd_*E11* | GTCCAGGCGCAAGAACAAAG |
| Rev_*E11* | GGTCACTGTTGACAAACCATCT |
| Fwd_*Wnt3a* | GGAGGGAGAAATGCCACTGTGTTT |
| Rev_*Wnt3a* | ACTTGCAGGTGTGCACGTCATAGA |
| Fwd_*GAPDH* | TCAGCAATGCCTCCTGCAC |
| Rev_*GAPDH* | TCTGGGTGGCAGTGATGGC |

### 2.9. Preparation of lamellae for transmission electron microscopy (TEM) analysis

The cell/collagen constructs were fixed using 2.5% glutaraldehyde, post-fixed in osmium tetroxide, and dehydrated as described earlier. The samples were then embedded in a Quetol-based resin by slow infiltration, followed by polymerization at 60 °C for 24 h. Ultrathin transverse sections (75-nm thickness) were cut using the diamond knife of a Leica EM UC7 ultra microtome and deposited onto the TEM copper grids. The sections were stained with uranyl acetate and lead citrate. The prepared TEM lamellae were analyzed using a JEOL 1400 transmission electron microscope and selected-area electron diffraction (SAED) patterns were obtained at 120 kV.

### 2.10. Raman spectroscopy analysis

The Raman spectroscopic technique was utilized to detect the maturation level of osteogenically differentiated cells, based on the extent of mineralized matrices reported in previous studies [22,23]. Spectra were obtained from the osteocytes cultured on coverslips with or without Wnt3a treatment using a WITec Alpha 300 series Raman Microscope (WITec GmbH, Ulm, Germany) equipped with a 785 nm-laser and a Zeiss 50× 0.7 NA objective. Wavenumber calibration was performed using the 520.5 $cm^{-1}$ band of a silicon wafer. For each experimental group, the collection time, typically 50 s, and laser power were adjusted to obtain an optimal signal-to-noise ratio [23]. Measurements were obtained from three individual sampling sites in each sample. The acquired raw spectra were corrected by subtracting the background fluorescence from the glass slide. The Raman peaks most significant to the classification process were identified. The biochemical correlates of these Raman peaks were also determined according to a previously published study [22].

### 2.11. Atomic Force Microscopy (AFM)

To obtain insights into the mechanical properties of the mineral nodules, the bonds between the minerals and collagen were analyzed using AFM (Supplementary Fig. 1) [24]. Samples were processed according to the protocol for SEM, but without the coating step. To calculate the level of mineral removal, images were recorded before and after the tip-surface force was applied to the mineralized substrate by an AFM probe during scanning. The Nanosurf FlexAFM (Nanosurf AG,

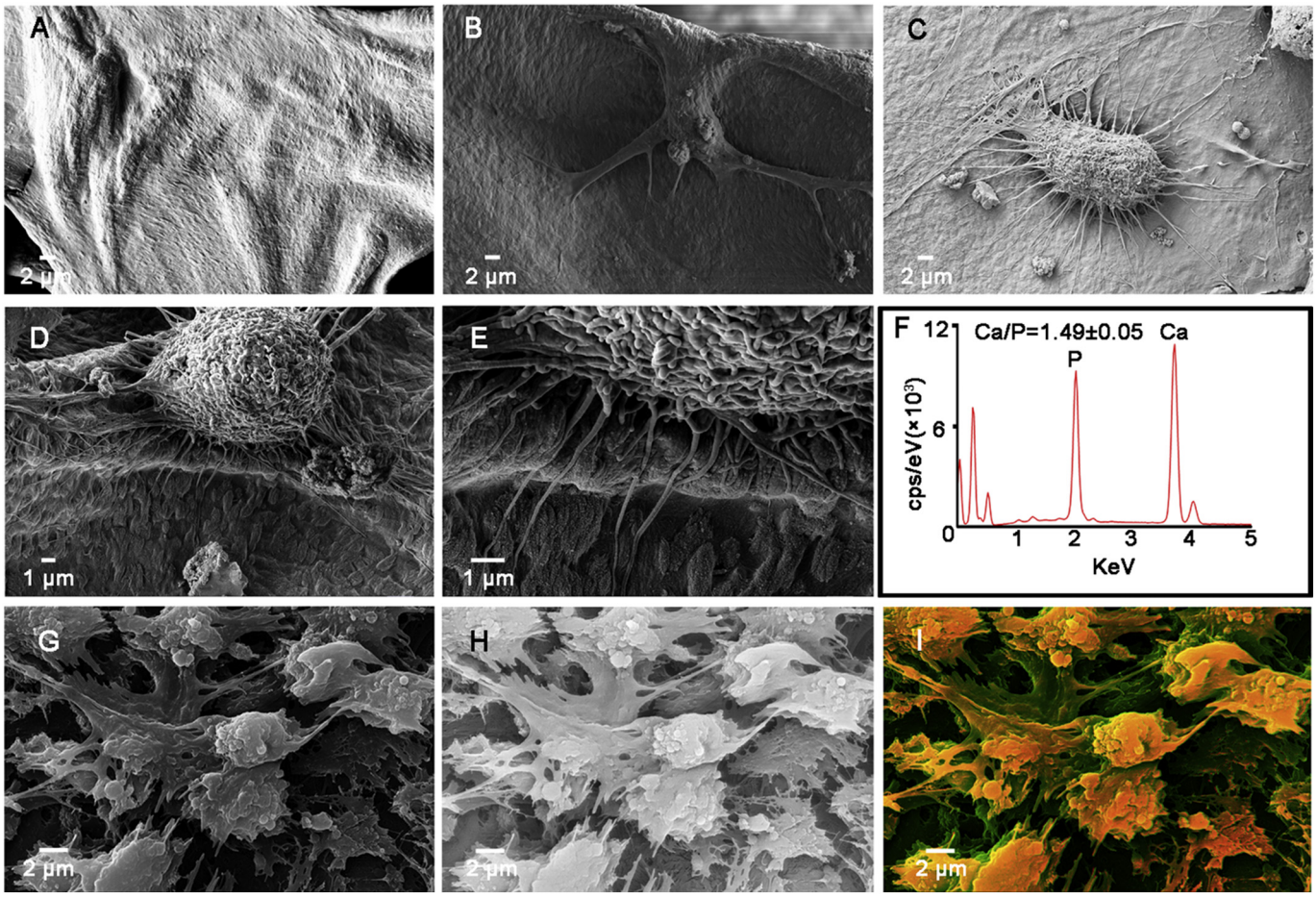


**Fig. 1.** In vitro osteocyte-mediated mineralization.
(A) General observation of the prefabricated collagen by SEM; Representative images of osteocytes maintained in (B) proliferation medium at 33 °C and (C) osteogenic medium at 37 °C for one week; (D and E) Representative enlarged SEM images of osteocytes in a two-week osteogenic culture maintained at 37 °C showing protruded dendritic processes; (F) Energy-dispersive X-ray spectroscopy (EDS) spectrum of mineralized collagen matrix presented in D and E; (G, H, and I) Image processing steps utilized to create the density–dependent color scanning electron micrographs (DDC-SEMs) of two-week osteogenic cultures maintained at 37 °C and identify dense spherical osteocyte cell bodies (orange/red) and a less dense surrounding matrix (green). (For interpretation of the references to color in this figure legend, the reader is referred to the web version of this article.)

Switzerland) and a rectangular cantilever were used. The cantilever had a pyramidal tip with a front angle of 9°. The cantilever spring constant was determined to be around 40.46 N/m. The sensitivity calibration, S, of the cantilever was performed by making indentations onto a hard surface to measure the slope of the force-height curve. The lateral detachment force was determined based on the total compression of the cantilever, probe geometry, and cantilever orientation. Additionally, the detachment forces required to achieve high, medium, and low levels of mineral removal, which were defined as 42%, 18%, and 8% removal, respectively, were recorded and statistically analyzed.

### 2.12. Animals and histological analysis

Catnb+/lox(exon 3) mice and dentin matrix protein 1 (DMP1)-Cre transgenic mice expressing Cre under the control of a 14-kb regulatory fragment of the gene DMP1 were maintained on a C57BL/6 background [25]. DMP1-Cre;β-catenin exon 3 fx+/+ or DMP1-Cre;β-catenin exon 3 fx+/− mice were the target mice in which β-catenin was constitutively activated in DMP1-positive cells, whereas the β-catenin exon 3 fx+/+ or β-catenin exon 3 fx+/− mice lacking DMP1-Cre were used as the controls. Six samples from the control and Wnt-activation groups were collected at postnatal weeks 2 and 7, respectively. They were then decalcified in 10% ethylenediaminetetraacetic acid (EDTA), and embedded in paraffin. Serial sections (5-μm-thick) were prepared for H&E and immunohistochemical staining against E11 (1:100; Invitrogen, catalogue# 14-5381-81), DMP1 (1:200) and SOST (1:100; both antibodies were kind gifts from Professor Jerry Feng of the Texas A &M University College of Dentistry).

### 2.13. Statistical analysis

All experiments were performed in triplicate for each condition and repeated thrice. All data were analyzed with the IBM SPSS software (SPSS Inc., Chicago, IL, USA). One-way analysis of variance (ANOVA) followed by Bonferroni post-hoc test was performed. Statistical significance was defined as $p \leq 0.05$.

## 3. Results

### 3.1. In vitro osteocyte-mediated mineralization

Collagen sponges were fabricated to demonstrate the ability of IDG-SW3 cells to infiltrate and mineralize 3D substrates. The general morphology of the prefabricated collagen was observed by SEM (Fig. 1A). Significantly more dendrites were shown to protrude from the osteocytes subjected to osteogenic differentiation for one week at 37 °C (Fig. 1C) than in osteocytes maintained in proliferation medium at 33 °C (Fig. 1B). Representative enlarged SEM images revealed that in a

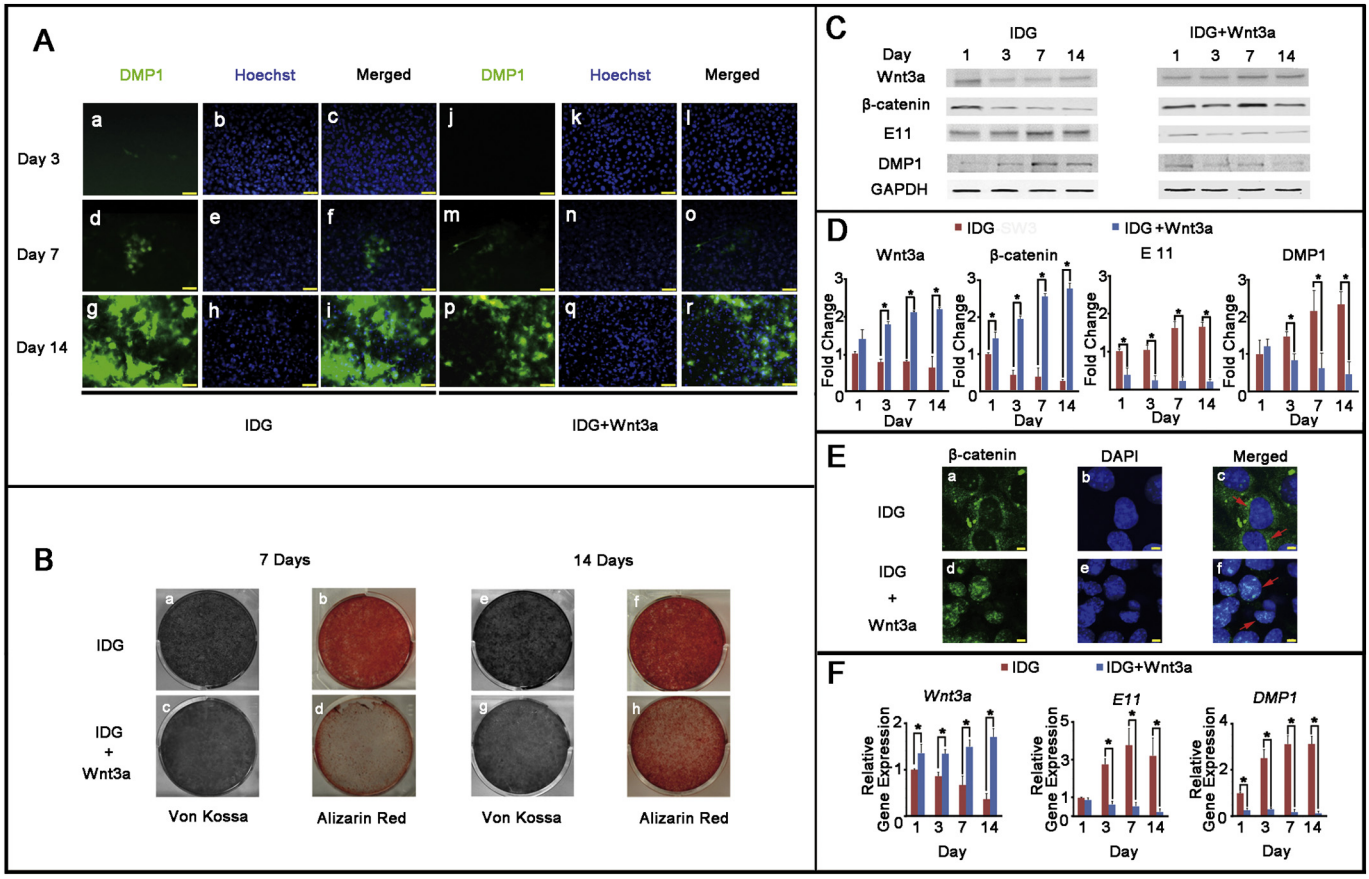


**Fig. 2.** Wnt/β-catenin signal activation disturbed mineralization and negatively affected the expression of osteocyte markers.
(A) The DMP1-GFP-positive cells during two weeks of osteogenic culture were imaged using fluorescence microscopy. (A-a, d, and g) The expression of DMP1 gradually increased in osteocytes after 14 days of osteogenic culture, (A-j, m, and p) whereas this GFP intensity decreased drastically when the cells were cultured with Wnt3a-supplemented medium. (A-b, e, h, k, n, and q) Cell nuclei were visualized using Hoechst 33342 staining. (A-c, f, i, l, o, and r) Merged images of DMP1 expression and cell nuclei at respective time points. Osteocytes and Wnt-activated osteocytes were subjected to osteogenic differentiation and the mineralization was observed by (B-a, c, e, and g) von Kossa staining and (B-b, d, f, and h) Alizarin Red S staining. A greater extent of mineralization was observed in normal osteocyte cultures on (B-e and f) day 14 compared to (B-a and b) day 7. The number of the nodules formed in Wnt-activated osteocytes were significantly reduced both on (B-c and d) day 7 and (B-g and h) day 14 compared to the normal osteocytes. (C) The representative western blotting images showed that the intensity of Wnt3a and β-catenin decreased gradually in osteocytes during 14 days of osteogenic culture, whereas the expression of E11 and DMP1 showed opposite trends. When the Wnt/β-catenin signaling was activated, the expression of E11 and DMP1 was observed to be significantly diminished with the elevated expression of the Wnt3a and β-catenin. (D) Quantitative analysis of the relative protein expression based on the western blotting results ($n = 3$, $^*p < 0.05$). (E) Immunofluorescence staining to confirm the active status of β-catenin (scale bar: 5 μm). (E-f, red arrows) In response to the Wnt stimulus, β-catenin was stabilized and translocated to the nucleus. (E-c, red arrows) In the two-week osteogenic cultures, β-catenin mainly expressed in the cytoplasm where it had no function. (F) A similar pattern was further confirmed at the gene transcription level (n = 3, $^*p < 0.05$). (For interpretation of the references to color in this figure legend, the reader is referred to the web version of this article.)

two-week osteogenic culture maintained at 37 °C, osteocytes were closely juxtaposed with the surrounding collagen (Fig. 1D and E), with dendritic processes extending inside the ECM. Elemental analysis revealed that the extracellular collagen matrix was mineralized with a calcium-to-phosphate (Ca/P) ratio close to that of carbonated apatite (Fig. 1F) [26]. Representative DDC-SEMs of two-week osteogenic cultures maintained at 37 °C show dense spherical osteocyte cell bodies (orange/red) and a less dense surrounding matrix (green) (Fig. 1G, H, and I); there appears to be an association between the organic matrix and the mineral.

### 3.2. Wnt/β-catenin signal activation disturbed bone mineralization and negatively affected the expression of osteocyte markers

The IDG-SW3 cells express GFP under the regulation of the DMP1 promoter. The fact that these cells can proliferate at 33 °C and differentiate into osteocytes at 37 °C makes these cells a powerful tool for osteocyte research. The DMP1-GFP-positive cells during two weeks of osteogenic culture were imaged using fluorescence microscopy (Fig. 2A-a to r). Under normal conditions, IDG-SW3 cells expressed GFP at a high intensity after 14 days of culture in osteogenic differentiation medium (Fig. 2A-a, d, and g). However, this GFP intensity decreased drastically over the course of two weeks of differentiation, when the cells were cultured with Wnt3a-supplemented medium (Fig. 2A-j, m, and p).

Alizarin Red S staining and von Kossa staining are essential for the initial investigation of the mineralized cultures, and these techniques were employed in the present study to examine the general mineralization during the osteogenic culturing of IDG-SW3 cells at 37 °C with or without Wnt/β-catenin signal activation. A large number of mineral nodules were formed by the IDG-SW3 cells after 7 days of osteogenic culture (Fig. 2B-a and b), and an even greater extent of mineralization was observed on day 14 (Fig. 2B-e and f). However, the number of the nodules formed in 7-day osteogenic cultures was significantly reduced in case of the IDG + Wnt3a group (Fig. 2B-c and d). Although by day 14, more mineralization was found in samples from the IDG + Wnt3a group (Fig. 2B-g and h) compared to the samples on day 7, a significantly reduced number of nodules was observed compared to the

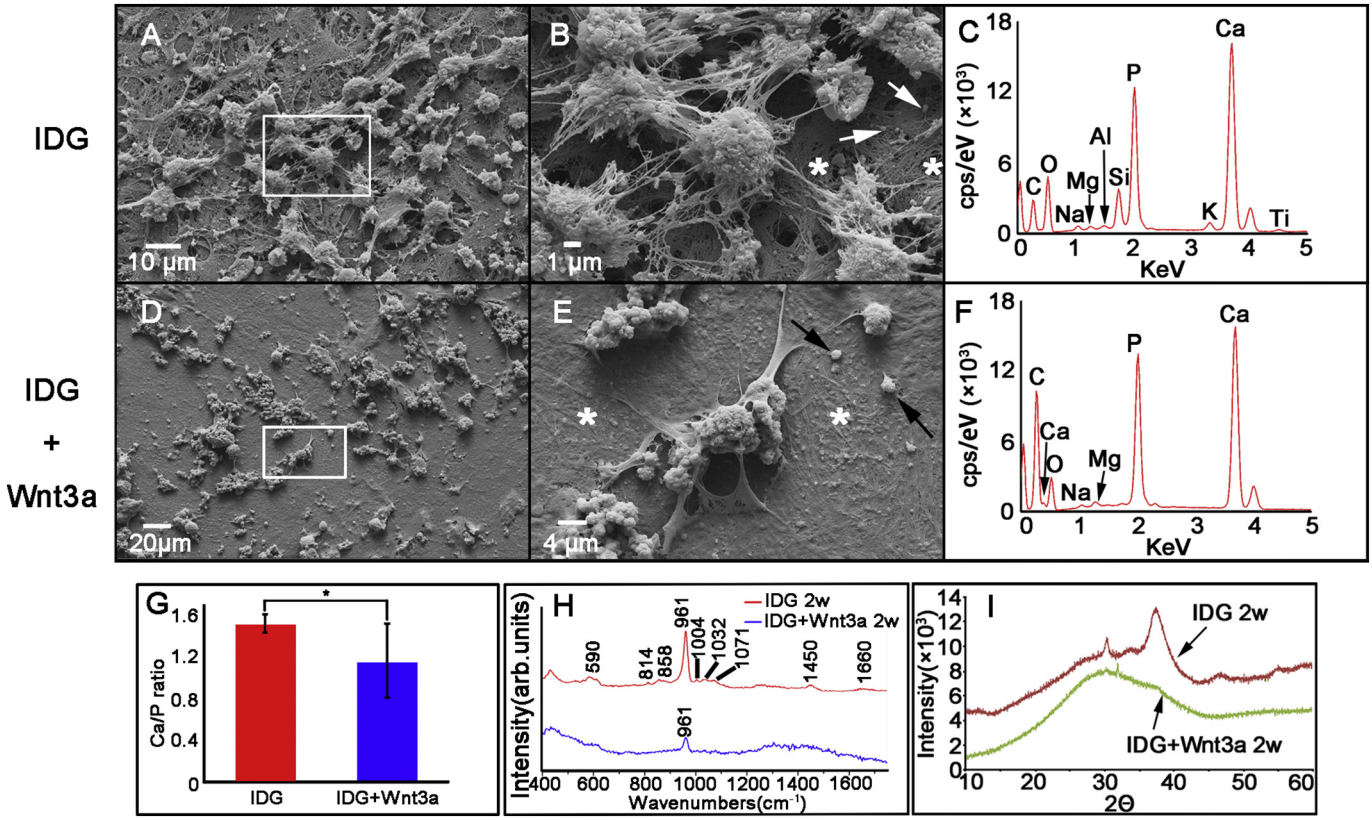


**Fig. 3.** Wnt/β-catenin signaling influenced ultrastructural morphology and composition of osteocyte mineralization.
(A and B) Representative SEM images revealed a continuous layer of mature osteocytes with numerous dendritic cell processes, (D and E) whereas membrane projections were barely seen in Wnt3a-activated osteocytes (Magnification: A, 3000×; B, 10,000×; D, 1000×; E, 5000×). (C, F, and G) The mineral particles produced by the IDG-SW3 cells showed a higher average calcium-to-phosphate (Ca/P) ratio than those produced by the Wnt3a-activated osteocytes. (H) Raman spectra collected from dense nodules, which were formed from normal osteogenic cultures, confirmed the presence of crystallized mineral particles. On the contrary, disappearance of the band at around 590 $cm^{-1}$ and the weak intensity of the peak at 961 $cm^{-1}$ in Wnt-activated osteocyte cultures indicate a spectrum similar to that of amorphous calcium phosphate and a decreased crystallinity in the mineral formations. (I) The X-ray diffraction (XRD) spectrum analysis showed that the crystal structures of the minerals formed in normal IDG-SW3 cultures were similar to those of the synthetic hydroxyapatite standard reference material, whereas the XRD spectrum of minerals from Wnt3a-activated osteocytes indicated that the particles were amorphous.

samples from the IDG group at day 14 (Fig. 2B-e and f).

The representative western blotting images showed that the intensity of Wnt3a and β-catenin decreased gradually in osteocytes during 14 days of osteogenic culture; however, the expression of E11, the earliest osteocyte marker, and DMP1, a critical marker of osteocytes expressed on the cell membrane, showed opposite trends (Fig. 2C). Interestingly, when the Wnt/β-catenin signaling was activated, the expression of E11 and DMP1 was observed to be significantly diminished with the elevated expression of the Wnt3a and β-catenin, as reflected in the quantitative analysis of the relative protein expression (Fig. 2D, $*p < 0.05$). In response to the Wnt stimulus, β-catenin was stabilized and translocated to the nucleus where it bound T-cell factor/lymphoid enhancer factor (TCF/LEF) to regulate the transcription of Wnt target genes as demonstrated by the immunofluorescence staining of β-catenin (Fig. 2E-f, red arrows). In the two-week osteogenic cultures, β-catenin mainly expressed in the cytoplasm (Fig. 2E-c, red arrows) where it had no function. A similar pattern was further confirmed at the gene transcription level (Fig. 2F). The constitutive activation of β-catenin in osteocytes increased the metaphyseal bone mass, as evidenced by the H&E staining (Supplementary Fig. 2A–D). Consistent with the *in vitro* findings, the genetically modified CA-β-catenin mice exhibited a diminished expression of E11 (Supplementary Fig. 2F), DMP1 (Supplementary Fig. 2J), and SOST (Supplementary Fig. 2N) at week 2. A decreased expression of DMP1 (Supplementary Fig. 2L) and SOST (Supplementary Fig. 2P), as well as an increased expression of E11 (Supplementary Fig. 2H) was found at week 7, suggesting that the activation of Wnt/β-catenin signaling may delay the protrusion of osteocyte dendrites and further restrict osteocyte maturation.

### 3.3. *Wnt/β-catenin signaling influenced the ultrastructural morphology and composition of osteocyte mineralization*

SEM analysis of the two-week osteogenic cultures grown on collagen-coated coverslips by revealed a continuous layer of mature osteocytes with numerous dendritic cell processes (Fig. 3A). The enlarged representative SEM image showed that multiple layers of osteocytes were embedded within, or were in close contact with the surrounding collagen matrix (Fig. 3B). The collagen matrix exhibited a strong association with the small calcospherites, which were evenly distributed among the collagen fibrils (Fig. 3B). In contrast, membrane projections were barely seen in Wnt3a-activated osteocytes, which presented as a non-continuous layer (Fig. 3D). At mineralization sites in the ECM, larger globular masses were randomly deposited on and in loose contact with the collagen fibrils (Fig. 3E). The large calcospherites coalesced and engulfed the localized collagen network during mineralization. Energy-dispersive X-ray microanalysis indicated the presence of minerals containing calcium and phosphorous associated with the globular structures and adjacent mineralized collagen fibrils. The mineral particles produced by the IDG-SW3 cells showed a higher average Ca/P ratio (Fig. 3C and G) than those produced by the Wnt3a-activated osteocytes (Fig. 3F and G). Raman spectra collected from dense nodules, which were formed from normal osteogenic cultures, showed a strong

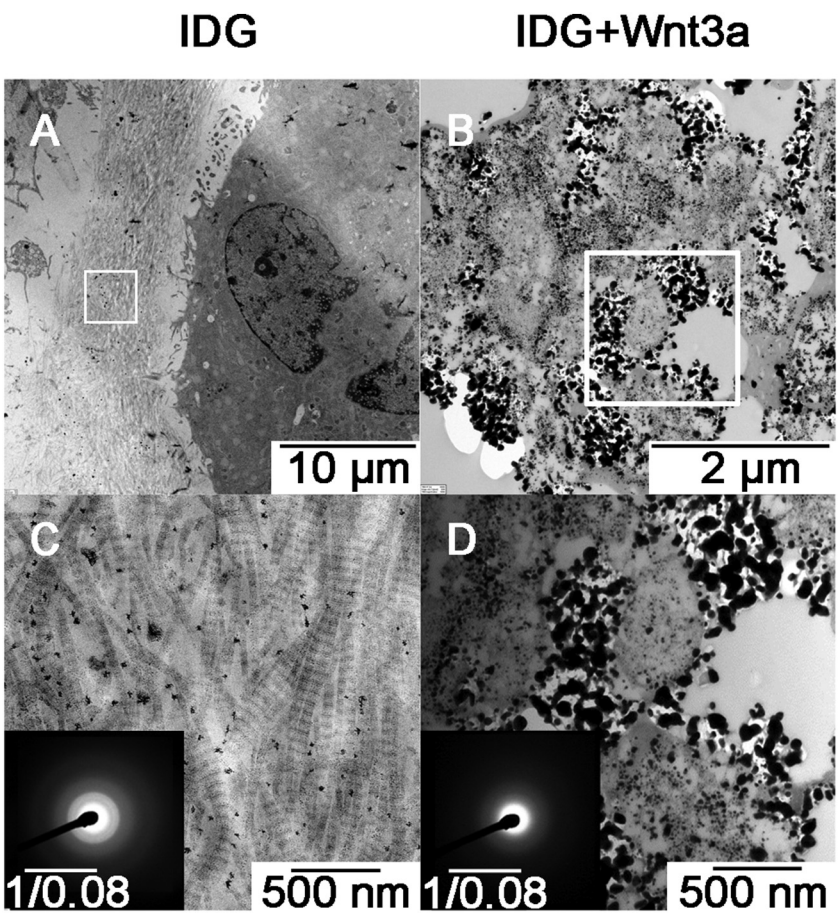


**Fig. 4.** Activation of Wnt/β-catenin signaling altered normal mineral crystallinity.
Representative TEM images revealed that the mineral nodules formed in (B and D) Wnt3a-activated osteocytes cultures were much larger in size with disordered morphologies and randomly deposited than (A and C) normal osteocyte cultures. Selected-area electron diffraction (SAED) patterns demonstrated a less distinctive diffraction ring in (D, inset) Wnt3a-activated osteogenic cultures compared to that in (C, inset) normal osteocyte cultures, suggesting that the crystal arrangement was negatively affected due to the activation of Wnt/β-catenin signaling.

peak associated with phosphate $\nu_1$ vibrations at 957 $cm^{-1}$, confirming the presence of crystallized mineral particles (Fig. 3H). The band observed at 590 $cm^{-1}$ corresponded to asymmetric and symmetric deformation modes of the γ4 $PO_4$ group, which could be used to identify the orientation of HA [27], and suggests a well-crystallized mineral formation. The weak peaks at 814 $cm^{-1}$, 858 $cm^{-1}$, and 1004 $cm^{-1}$ could be related to the collagen matrix [28]. The matrix vesicles also showed a small and sharp band at 1004 $cm^{-1}$. The peak at 858 $cm^{-1}$ could represent nucleic acids in the spectra [29]. The broad weak band at 1071 $cm^{-1}$ corresponded to the carbonate ($CO_3^{2-}$) $\nu$1 symmetric stretch [30,31]. The peak at 1660 $cm^{-1}$ was indicative of the amide I band. Differences in the spectral signatures of the mineralized materials following Wnt3a activation are clearly visible; disappearance of the band at around 590 $cm^{-1}$ and the weak intensity of the peak at 961 $cm^{-1}$ indicate a spectrum similar to that of amorphous calcium phosphate (ACP) and a decreased crystallinity in the mineral formations. The crystal structure of the minerals formed in the IDG-SW3 cell cultures was assessed by X-ray diffraction (XRD) and compared to a synthetic hydroxyapatite standard reference material (HA-SRM). As shown in Fig. 3I, the minerals in the osteogenically differentiated IDG-SW3 cell culture showed diffraction peaks at 2θ values of 30.2° and 37.08°, corresponding to hydroxyapatite (ICCD No. 9-432), for the *hlk* values 121 and 211, respectively. The broad bands indicated an XRD pattern characteristic of a somewhat crystallized apatite material, typical of that reported for biologic apatites, with 2θ positions matching those of a carbonated hydroxyapatite phase. In contrast, the XRD spectrum of minerals from Wnt3a-activated osteocytes exhibited a smooth wave line without any protuberance, indicating that the particles were amorphous.

### *3.4. Activation of Wnt/β-catenin signaling altered normal mineral crystallinity*

TEM imaging of the ultrathin sections of mineralized osteocyte cultures revealed that under conditions of normal mineralization, osteocytes were closely juxtaposed to the collagen fibrils of the ECM, and attached with numerous small mineral particles (Fig. 4A). In contrast, cell organelles of Wnt-activated osteocytes were not distinctive, and the mineral nodules were much larger in size and randomly deposited (Fig. 4B). The enlarged TEM image of cultures with normal mineralization showed that the densely packed bundles of collagen fibrils displayed the characteristic banding periodicity typical of type I collagen fibrils (Fig. 4C). The mineral particles in normal mineralized cultures were arrayed along the long axis of the collagen fibrils. In contrast, more mineral particles in Wnt3a-activated cultures merged and coalesced into larger aggregates, revealing globular accumulations with disordered morphologies (Fig. 4D). No collagen fibrils were identified in case of the Wnt-activated osteocytes. Electron-dense mineral particles were evident within cells; they were present within membrane invaginations and immediately outside plasma membranes. The crystal orientation of the mineral precipitates was further examined by SAED to elucidate the arrangement of the minerals. Electron diffraction patterns of normal osteogenically differentiated IDG-SW3 cells demonstrated crystalline textures, which resembled those from native mineralized tissues, where the arcs corresponded to spaced (211), (112), and (310) planes (Fig. 4C, inset). On the other hand, the electron diffraction patterns of Wnt3a-activated osteogenic cultures showed a less distinctive diffraction ring, which was quite similar to that of biological ACP (Fig. 4D, inset), suggesting that the crystal arrangement was negatively affected due to the activation of Wnt/β-catenin signaling.

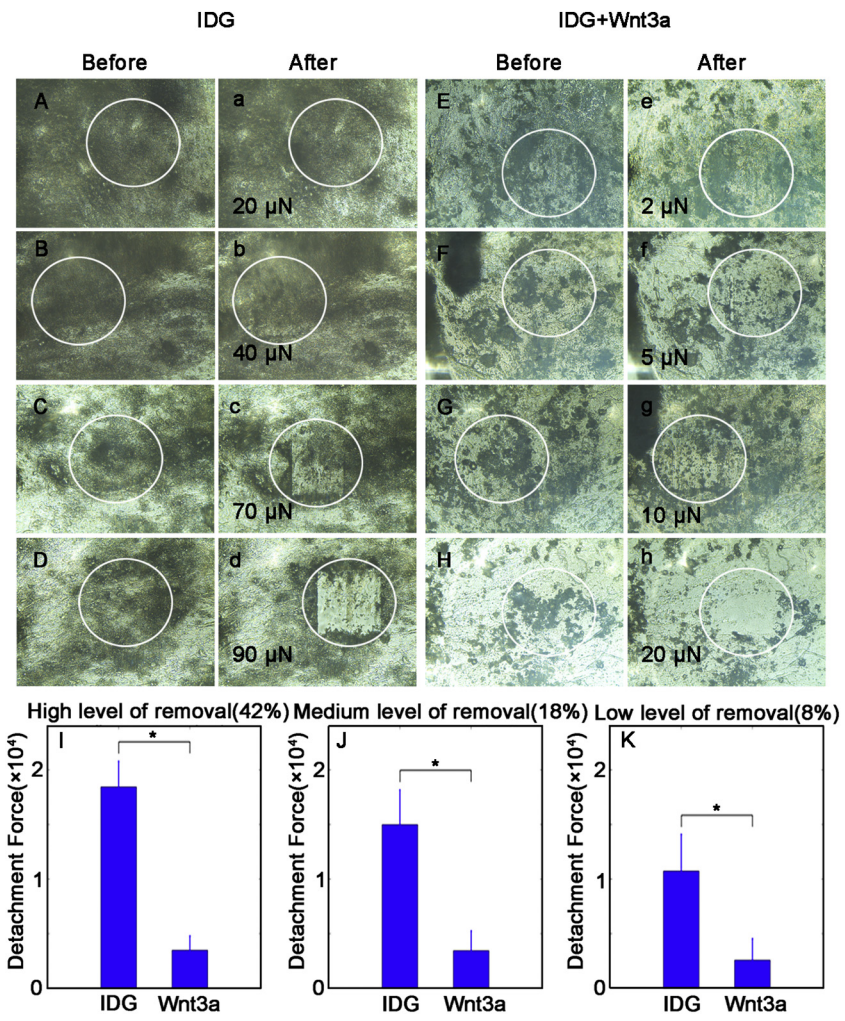


**Fig. 5.** Activation of Wnt/β-catenin signaling impaired the mechanical properties of mineralization.
Representative microscope images captured in the same area (A–D and E–H) before and (a–d and e–h) after the application of AFM cantilever to remove minerals demonstrated a generally higher detachment force was needed for mineral removal in normal osteocyte cultures, compared to Wnt-activated osteocyte cultures. Three levels of mineral nodule removal were established according to the percentage of mineral nodules removed: high (42%), medium (18%), and low (8%), respectively. (I–K) Significantly stronger detachment forces were required for removing mineral nodules to achieve all three removal levels in IDG-SW3 cells showing normal mineralization, which indicates that normal mineral nodules are bound more tightly to collagen.

### *3.5. Wnt/β-catenin signaling impaired the mechanical properties of mineralization*

The mechanical property of tissue mineralization is critical for bone function; hence, this study utilized AFM to investigate the bonding force of the nodules formed in the osteogenic cultures with or without the supplementation of Wnt3a. Almost no nodules could be removed in the normal group after a detachment force of 20 μN was applied (Fig. 5A and a); however, a greater number of nodules were evidently removed when the detachment force was increased to 40 μN and 70 μN (Fig. 5B–C and b–c). Removing most of the nodules in the normal group required a detachment force as high as 90 μN (Fig. 5D and d). On the contrary, most nodules were removed in cultures from the Wnt3a-treated group after a force of 2 μN was applied (Fig. 5E and e), although higher detachment forces also led to increasing levels of mineral nodule removal (Fig. 5F–H and f–h). For quantitative analysis, three levels of mineral nodule removal were established according to the percentage of mineral nodules removed: high (42%), medium (18%), and low (8%). Significantly stronger detachment forces were required for removing mineral nodules to achieve all three removal levels in IDG-SW3 cells showing normal mineralization, which indicates that normal mineral nodules are bound more tightly to collagen (Fig. 5I–K).

## 4. Discussion

Bone mineralization, which is a controlled and tightly regulated process, is achieved by the deposition of hydroxyapatite nanocrystals in collagen fibrils and the interplay of the collagen matrix and non-collagenous proteins [32]. Studying the process of bone mineralization is challenging due to the difficulty in accessing the mineral-forming sites in living organisms and the shifting of the mineralization front as mineralization proceeds with time. This has necessitated a reliance on cell culture models to understand the molecular process of mineralization and the mechanisms underlying this process. Recently, a thorough characterization of the mineralization process in the murine MC3T3-E1 pre-osteoblast cell culture model has been reported; many key similarities with regards to the structure and composition of the biominerals and mineralization processes have been observed between this cell line and normal bone tissues [33]. However, as osteoblasts are located far away from the mineralization frontline, recent studies have suggested that osteoid osteocytes have a more important role in the mineralization process [34,35]. Osteocytes, the cells residing within the bone matrix, have long been considered “passive place holders” in bones [3]. However, recently, it has been recognized that osteocytes act as major orchestrators of skeletal activity, capable of sensing and integrating mechanical and chemical signals to regulate both bone formation and resorption [36].

Accumulating evidence has suggested that canonical Wnt/β-catenin signaling plays a dominant role in bone homeostasis and exerts cell context-dependent functions on osteoblastic cells depending on the stage of differentiation. It has been reported that the activation of the Wnt/β-catenin pathway in mesenchymal progenitors and osteoblast-committed precursors accelerates osteoblast differentiation and bone formation [37,38], whereas the inhibition of Wnt signaling leads to the arrest of osteoblast differentiation [39]. Osteocyte-specific β-catenin-deficient mice present with a low-bone-mass phenotype, which is

probably due to increased osteoclast number and activity [14]. However, activation of osteocytic β-catenin signaling has been reported to increase the numbers of both osteoclasts and osteoblasts, leading to bone gain [40]; however, other findings have shown that the constitutive activation of β-catenin in osteocytes results in inferior bone strength and bone growth [15].

Dysregulated activation of Wnt during the late osteogenic differentiation stage, as presented in our study, can lead to altered osteocyte morphology and decreased expression of specific proteins secreted by osteocytes, including DMP1. Since DMP1 is a highly acidic, phosphorylated, extracellular, and non-collagenous protein [41] belonging to the small integrin-binding ligand N-linked glycoprotein (SIBLINGs) protein family [42], its role in proper bone mineralization is critical, *i.e.*, DMP1 helps minerals infiltrate into collagen fibrils [43,44]. Our study demonstrates that the activation of the Wnt/β-catenin pathway in osteocytes can lead to a decreased expression of DMP1, and eventually, a poor integration of collagen and minerals. The abnormal elemental signature of the Wnt-activated osteocyte cultures compared to that of the normal osteogenic cultures, together with reduced crystallinity (as shown in the XRD spectrum), suggest that Wnt signal activation inhibits the formation of highly crystallized calcium phosphate in osteocytes. The minerals in the osteocyte cultures were identified as carbonated HA, in accordance with the obtained Raman spectrum. Compared to the single peak in Wnt-activated osteocyte cultures, the weak peaks at 814 $cm^{-1}$, 858 $cm^{-1}$,1004 $cm^{-1}$, and 1660 $cm^{-1}$ in the normal osteocyte cultures indicate the bonding between collagen and HA, suggesting an active bone mineral metabolism, whereas Wnt-activated osteocytes may produce calcium phosphate molecules that do not integrate with the matrix. This was confirmed by the TEM results, which showed the integration of collagen fibrils and HA crystals in samples from the normal group, whereas the mineral deposits were shown to enwrapped coat the cells without binding with collagen in the Wnt-activated osteocyte cultures. This negatively affects the normal mineral crystallinity, with ACP not being properly converted to crystalline hydroxyapatite, and further contributes to the impaired mechanical property of mineralized nodules; this may explain the abnormal phenotype observed in osteocyte-specific CA-β-catenin mice [15].

Collectively, by using the IDG-SW3 cell line as an *in vitro* model, this study demonstrates that osteocyte-specific β-catenin activation can lead to decreased expression of DMP1, which further contributes to the impaired composition, structure, and mechanical properties of the mineralized products.

Supplementary data to this article can be found online at https://doi.org/10.1016/j.bone.2019.06.027.

## Acknowledgement

This work was supported by the Science and Technology Project Grants, Xiamen Science and Technology Bureau (Grant No. 3502Z20161247), the National Health and Medical Research Council (NHMRC) Early Career Fellowship (Grant No. 1105035), the National Natural Science Foundation of China (NSFC) General Project (Grant No. 31771025), and the NSFC Young Scientists Fund (Grant No. 81700969). The authors would like to acknowledge the facilities, and the scientific and technical assistance of Dr. Jamie Riches and Ms. Ning Liu of the Australian Microscopy & Microanalysis Research Facility at the Central Analytical Research Facility operated by the Institute for Future Environments at the Queensland University of Technology. The authors would also like to acknowledge the animal samples and antibodies kindly provided by Professor Jerry Feng of the Texas A&M University College of Dentistry.

## References

[1] E.M. Aarden, E.H. Burger, P.J. Nijweide, Function of osteocytes in bone, J. Cell. Biochem. 55 (3) (1994) 287–299.
[2] S.L. Dallas, M. Prideaux, L.F. Bonewald, The osteocyte: an endocrine cell ... and more, Endocr. Rev. 34 (5) (2013) 658–690.
[3] L.F. Bonewald, The amazing osteocyte, J. Bone Miner. Res. 26 (2) (2011) 229–238.
[4] S.M. Woo, J. Rosser, V. Dusevich, I. Kalajzic, L.F. Bonewald, Cell line IDG-SW3 replicates osteoblast-to-late-osteocyte differentiation in vitro and accelerates bone formation in vivo, J. Bone Miner. Res. 26 (11) (2011) 2634–2646.
[5] G. Rawadi, B. Vayssiere, F. Dunn, R. Baron, S. Roman-Roman, BMP-2 controls alkaline phosphatase expression and osteoblast mineralization by a Wnt autocrine loop, J. Bone Miner. Res. 18 (10) (2003) 1842–1853.
[6] E. Jarvinen, I. Salazar-Ciudad, W. Birchmeier, M.M. Taketo, J. Jernvall, I. Thesleff, Continuous tooth generation in mouse is induced by activated epithelial Wnt/beta-catenin signaling, Proc. Natl. Acad. Sci. U. S. A. 103 (49) (2006) 18627–18632.
[7] S. Kang, C.N. Bennett, I. Gerin, L.A. Rapp, K.D. Hankenson, O.A. Macdougald, Wnt signaling stimulates osteoblastogenesis of mesenchymal precursors by suppressing CCAAT/enhancer-binding protein alpha and peroxisome proliferator-activated receptor gamma, J. Biol. Chem. 282 (19) (2007) 14515–14524.
[8] T.P. Hill, D. Spater, M.M. Taketo, W. Birchmeier, C. Hartmann, Canonical Wnt/beta-catenin signaling prevents osteoblasts from differentiating into chondrocytes, Dev. Cell 8 (5) (2005) 727–738.
[9] S.L. Etheridge, G.J. Spencer, D.J. Heath, P.G. Genever, Expression profiling and functional analysis of wnt signaling mechanisms in mesenchymal stem cells, Stem Cells 22 (5) (2004) 849–860.
[10] V.S. Salazar, S. Ohte, L.P. Capelo, L. Gamer, V. Rosen, Specification of osteoblast cell fate by canonical Wnt signaling requires Bmp2, Development 143 (23) (2016) 4352–4367.
[11] H. Hu, M.J. Hilton, X. Tu, K. Yu, D.M. Ornitz, F. Long, Sequential roles of Hedgehog and Wnt signaling in osteoblast development, Development 132 (1) (2005) 49–60.
[12] S.L. Holmen, C.R. Zylstra, A. Mukherjee, R.E. Sigler, M.C. Faugere, M.L. Bouxsein, L. Deng, T.L. Clemens, B.O. Williams, Essential role of beta-catenin in postnatal bone acquisition, J. Biol. Chem. 280 (22) (2005) 21162–21168.
[13] D.A. Glass 2nd, P. Bialek, J.D. Ahn, M. Starbuck, M.S. Patel, H. Clevers, M.M. Taketo, F. Long, A.P. McMahon, R.A. Lang, G. Karsenty, Canonical Wnt signaling in differentiated osteoblasts controls osteoclast differentiation, Dev. Cell 8 (5) (2005) 751–764.
[14] I. Kramer, C. Halleux, H. Keller, M. Pegurri, J.H. Gooi, P.B. Weber, J.Q. Feng, L.F. Bonewald, M. Kneissel, Osteocyte Wnt/beta-catenin signaling is required for normal bone homeostasis, Mol. Cell. Biol. 30 (12) (2010) 3071–3085.
[15] S. Chen, J. Feng, Q. Bao, A. Li, B. Zhang, Y. Shen, Y. Zhao, Q. Guo, J. Jing, S. Lin, Z. Zong, Adverse effects of osteocytic constitutive activation of β-catenin on bone strength and bone growth, J. Bone Miner. Res. 30 (7) (2015) 1184–1194.
[16] E.J. Miller, R.K. Rhodes, Preparation and characterization of the different types of collagen, Methods Enzymol. 82 (1982) 33–64.
[17] S. Li, J. Shao, Y. Zhou, T. Friis, J. Yao, B. Shi, Y. Xiao, The impact of Wnt signalling and hypoxia on osteogenic and cementogenic differentiation in human periodontal ligament cells, Mol. Med. Rep. 14 (6) (2016) 4975–4982.
[18] P. Han, S. Ivanovski, R. Crawford, Y. Xiao, Activation of the canonical Wnt signaling pathway induces cementum regeneration, J. Bone Miner. Res. 30 (7) (2015) 1160–1174.
[19] Y. Zhou, W. Fan, I. Prasadam, R. Crawford, Y. Xiao, Implantation of osteogenic differentiated donor mesenchymal stem cells causes recruitment of host cells, J. Tissue Eng. Regen. Med. 9 (2) (2015) 118–126.
[20] Y. Zhou, R. Huang, W. Fan, I. Prasadam, R. Crawford, Y. Xiao, Mesenchymal stromal cells regulate the cell mobility and the immune response during osteogenesis through secretion of vascular endothelial growth factor A, J. Tissue Eng. Regen. Med. 12 (1) (2018) e566–e578.
[21] S. Bertazzo, E. Gentleman, K.L. Cloyd, A.H. Chester, M.H. Yacoub, M.M. Stevens, Nano-analytical electron microscopy reveals fundamental insights into human cardiovascular tissue calcification, Nat. Mater. 12 (6) (2013) 576–583.
[22] P.S. Hung, Y.C. Kuo, H.G. Chen, H.H. Chiang, O.K. Lee, Detection of osteogenic differentiation by differential mineralized matrix production in mesenchymal stromal cells by Raman spectroscopy, PLoS One 8 (5) (2013) e65438.
[23] A.A. Volponi, E. Gentleman, R. Fatscher, Y.W. Pang, M.M. Gentleman, P.T. Sharpe, Composition of mineral produced by dental mesenchymal stem cells, J. Dent. Res. 94 (11) (2015) 1568–1574.
[24] T.D. Nguyen, Y. Gu, Investigation of cell-substrate adhesion properties of living chondrocyte by measuring adhesive shear force and detachment using AFM and inverse FEA, Sci. Rep. 6 (2016) 38059.
[25] J.Q. Feng, E.L. Clinkenbeard, B. Yuan, K.E. White, M.K. Drezner, Osteocyte regulation of phosphate homeostasis and bone mineralization underlies the pathophysiology of the heritable disorders of rickets and osteomalacia, Bone 54 (2) (2013) 213–221.
[26] B. Wopenka, J.D. Pasteris, A mineralogical perspective on the apatite in bone, Mat Sci Eng C-Bio S 25 (2) (2005) 131–143.
[27] H. Tsuda, J. Arends, Orientational micro-Raman spectroscopy on hydroxyapatite single crystals and human enamel crystallites, J. Dent. Res. 73 (11) (1994) 1703–1710.
[28] J.J. Freeman, B. Wopenka, M.J. Silva, J.D. Pasteris, Raman spectroscopic detection of changes in bioapatite in mouse femora as a function of age and in vitro fluoride treatment, Calcif. Tissue Int. 68 (3) (2001) 156–162.
[29] L.L. McManus, F. Bonnier, G.A. Burke, B.J. Meenan, A.R. Boyd, H.J. Byrne, Assessment of an osteoblast-like cell line as a model for human primary osteoblasts using Raman spectroscopy, Analyst 137 (7) (2012) 1559–1569.
[30] A.F. Khan, M. Awais, A.S. Khan, S. Tabassum, A.A. Chaudhry, I.U. Rehman, Raman spectroscopy of natural bone and synthetic apatites, Appl. Spectrosc. Rev. 48 (4) (2013) 329–355.
[31] P.E. Timchenko, E.V. Timchenko, E.V. Pisareva, M.Y. Vlasov, N.A. Red'kin,

O.O. Frolov, Spectral analysis of allogeneic hydroxyapatite powders, J. Phys. Conf. Ser. 784 (2017).
[32] J.P. Gorski, Biomineralization of bone: a fresh view of the roles of non-collagenous proteins, Front Biosci (Landmark Ed) 16 (2011) 2598–2621.
[33] W.N. Addison, V. Nelea, F. Chicatun, Y.C. Chien, N. Tran-Khanh, M.D. Buschmann, S.N. Nazhat, M.T. Kaartinen, H. Vali, M.M. Tecklenburg, R.T. Franceschi, M.D. McKee, Extracellular matrix mineralization in murine MC3T3-E1 osteoblast cultures: an ultrastructural, compositional and comparative analysis with mouse bone, Bone 71 (2015) 244–256.
[34] Y. Mikuni-Takagaki, Y. Kakai, M. Satoyoshi, E. Kawano, Y. Suzuki, T. Kawase, S. Saito, Matrix mineralization and the differentiation of osteocyte-like cells in culture, J. Bone Miner. Res. 10 (2) (1995) 231–242.
[35] Y.B. Lu, B.Z. Yuan, C.L. Qin, Z.G. Cao, Y.X. Xie, S.L. Dallas, M.D. Mckee, M.K. Drezner, L.F. Bonewald, J.Q. Feng, The biological function of DMP-1 in osteocyte maturation is mediated by its 57-kDa C-terminal fragment, J. Bone Miner. Res. 26 (2) (2011) 331–340.
[36] M.B. Schaffler, W.Y. Cheung, R. Majeska, O. Kennedy, Osteocytes: master orchestrators of bone, Calcif. Tissue Int. 94 (1) (2014) 5–24.
[37] S. Minear, P. Leucht, J. Jiang, B. Liu, A. Zeng, C. Fuerer, R. Nusse, J.A. Helms, Wnt proteins promote bone regeneration, Sci. Transl. Med. 2 (29) (2010) 29ra30.
[38] S.X. Cai, A.R. Liu, S. Chen, H.L. He, Q.H. Chen, J.Y. Xu, C. Pan, Y. Yang, F.M. Guo, Y.Z. Huang, L. Liu, H.B. Qiu, Activation of Wnt/beta-catenin signalling promotes mesenchymal stem cells to repair injured alveolar epithelium induced by lipopolysaccharide in mice, Stem Cell Res Ther 6 (2015).
[39] T.F. Day, X. Guo, L. Garrett-Beal, Y. Yang, Wnt/beta-catenin signaling in mesenchymal progenitors controls osteoblast and chondrocyte differentiation during vertebrate skeletogenesis, Dev. Cell 8 (5) (2005) 739–750.
[40] X. Tu, J. Delgado-Calle, K.W. Condon, M. Maycas, H. Zhang, N. Carlesso, M.M. Taketo, D.B. Burr, L.I. Plotkin, T. Bellido, Osteocytes mediate the anabolic actions of canonical Wnt/beta-catenin signaling in bone, Proc. Natl. Acad. Sci. U. S. A. 112 (5) (2015) E478–E486.
[41] A. George, B. Sabsay, P.A. Simonian, A. Veis, Characterization of a novel dentin matrix acidic phosphoprotein. Implications for induction of biomineralization, J. Biol. Chem. 268 (17) (1993) 12624–12630.
[42] A. Bellahcene, V. Castronovo, K.U. Ogbureke, L.W. Fisher, N.S. Fedarko, Small integrin-binding ligand N-linked glycoproteins (SIBLINGs): multifunctional proteins in cancer, Nat. Rev. Cancer 8 (3) (2008) 212–226.
[43] K. Narayanan, A. Ramachandran, J. Hao, G. He, K.W. Park, M. Cho, A. George, Dual functional roles of dentin matrix protein 1. Implications in biomineralization and gene transcription by activation of intracellular Ca2+ store, J. Biol. Chem. 278 (19) (2003) 17500–17508.
[44] G. He, S. Gajjeraman, D. Schultz, D. Cookson, C.L. Qin, W.T. Butler, J.J. Hao, A. George, Spatially and temporally controlled biomineralization is facilitated by interaction between self-assembled dentin matrix protein 1 and calcium phosphate nuclei in solution, Biochemistry-Us 44 (49) (2005) 16140–16148.